Improving Cable Driven Parallel Robot Accuracy Through Angular Position Sensors

Article · December 2016

DOI: 10.1109/IROS.2016.7759640

3 authors:

Alexis Fortin-Cote
Laval University
8 PUBLICATIONS **8** CITATIONS
SEE PROFILE

Philippe Cardou
Laval University
61 PUBLICATIONS **433** CITATIONS
SEE PROFILE

Alexandre Campeau-Lecours
Laval University
44 PUBLICATIONS **181** CITATIONS
SEE PROFILE

Improving Cable Driven Parallel Robot Accuracy Through Angular Position Sensors

This paper is a Post-Print version (ie final draft post-refereeing). For access to Publisher's version, please access http://ieeexplore.ieee.org/document/7759640

IEEE/RSJ 2016.

Alexis Fortin-Côté, Philippe Cardou and Alexandre Campeau-Lecours

***Abstract*— Conventionally, a cable driven parallel mechanism (CDPM) pose is obtained through the forward kinematics from measurements of the cable lengths. However, this estimation method can be limiting for some applications requiring more precision. This paper proposes to use cable angle position sensors in addition to cable length measurements in order to improve the accuracy of such mechanisms. The robot pose is first obtained individually by the cable length measurements and the cable angle position measurements. A data fusion scheme combining these two types of measurements is then proposed in order to improve the CPDM accuracy. Finally, simulations and experiments are presented in order to assess the benefits of using cable angle position sensors on the CDPM.**

I. INTRODUCTION

Cable driven parallel mechanisms research has seen a growing interest in the last two decades. Their implementation as an alternative to rigid-link parallel mechanisms such as the Gough-Stewart platform for applications needing larger workspace has grown with developments in area such as haptics [1], motion simulator, material handling, 3D printing and maintenance [2]. As opposed to conventional rigid links mechanisms, CDPMs are known to admit larger workspace with a relatively low inertia. The Skycam [3] and (a version of) the RobotCrane [4] used to remove paint on military aircraft are good examples of CDPMs with large workspace used in commercial applications. Increasing workspace comes with new challenges in terms of position accuracy. Conventionally, the CDPM pose is obtained through the forward kinematics by using a measurement of the cable length as input. This method has proven satisfactory for a number of applications, but can be limiting in application requiring more precision. This paper proposes to use cable-angle position sensors in addition to cable length measurements in order to improve the accuracy of such mechanisms. Some research has been done on the accuracy of CDPMs [5], but none, to the knowledge of the authors, employ angular position sensors. Measurement redundancy of parallel robots for calibration has been proposed in the literature with additional length sensors [6], but not for angular sensors. Measurement redundancy with angular sensors has also been proposed for parallel robots [7], but as a means of solving the forward kinematic in a closed form. Another solution to improve forward kinematic accuracy is to use external vision sensor [8], [9]. Vision based sensor and hefty cable model are in the control scheme to achieve better positional accuracy. The drawback of this method is the cost and encumbrance of the camera system.

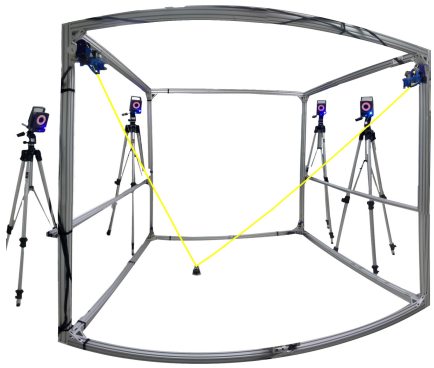

Fig. 1: Photograph of the CDPM and sensors used in this work.

The simplification of massless and rigid cable is used in this paper. While this is a common simplification in the cable robot literature, it is important to verify its validity. Nguyen and al. [10] assess the validity of some of those simplifications in computing the forward kinematic. Kraus and al. [11] added elasticity to their model and saw an increase of up to 50% in accuracy of the forward kinematic. The validity of the simplification is assessed in sec.VI.

In this paper, the main objective of using angular sensors in conjunction with typical cable length sensor is to increase the accuracy of the CDPM pose estimate. The hypothesis is that using both the cable length measurement and the angular measurement in a sensor fusion scheme would lead to an increased accuracy. For instance, the angular information could increase the accuracy when the cable length measurement have a low kinematic sensitivity [12], e.g. where large end-effector movements results in small changes in length.

This paper is structured as follows. The angular sensor is

*This work was supported by the Natural Sciences and Engineering Research Council of Canada (NSERC) and by the Canada Research Chair program.

The authors are with the Laboratoire de robotique, Département de génie mécanique, Université Laval, Québec, Canada, G1V 0A6 alexis.fortin-cote.1@ulaval.ca and cardou@gmc.ulaval.ca and alexandre.campeau-lecours@gmc.ulaval.ca

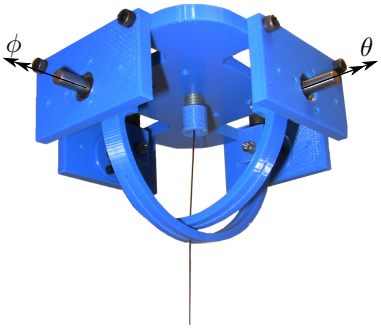

Fig. 2: The angular position sensors proposed in this work with the measured axis displayed.

first presented. Then, the kinematic equations of a general CDPM are independently obtained with the cable length as input and with the angular position measure as input. A fusion algorithm using both inputs is then developed to obtain an estimation of the pose. A simulation using a planar two-degree-of-freedom CDPM, as that shown in Fig. 1, is then presented to asses the theoretic improvement on accuracy by comparing the independent pose estimation and the sensor fusion estimation. Finally, an experiment is performed to assess the practical difference on the accuracy.

II. Angular Position Sensor

In more traditional applications, the CDPM cable lengths are measured by using sensors such as encoders similarly to the FALCON [13], the INCA6D [14], the ReelAx [15]. However, measuring the angle of departure of the cable in three-dimensional space is a more involved problem to which different solutions have been proposed in the literature. Amongst them are a non-contact sensor using the magnetic field [16], accelerometers based inclinometers [17], machine vision [18], [19], a cardan-based mechanism [20], a linear cable displacement sensor [21] and observer based solutions [22]. The angular position sensor used in this work [23], [24] has been developed to be robust, accurate, simple and low cost. A contact sensor using encoders was preferred since it represents a proven and robust solution in the industry. Amongst existing contact based sensors, Cardan based mechanisms [20] and sensors detecting the horizontal displacement of the cable [21] could also be used. However, their design implementation inherently limits the precision and achievable workspace.

The sensor used in this work is a two-degree-of-freedom (DOF) angular position sensor as shown in Fig. 2. It consists of two concentric grooved guides which are driven by the cable as it passes through them. Both axes of rotation of the guides are intersecting at the origin point of the cable. Fig. 2 shows the axes, θ and ϕ, about which the angles are measured. The two guides are independent from each other and rotate about orthogonal axes thus allowing the measurement of two independent angles. The cable angular positions are obtained by rotational encoders affixed to both cable guides. A lightweight construction and the use of ball bearings limit the interaction forces between the cable and the guides.

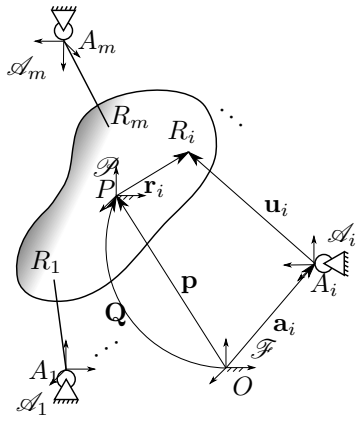

Fig. 3: Geometric model of a generic cable driven parallel mechanism.

III. Kinematics

In this section the kinematic equations of a cable based mechanism are developed, both by considering measurements of the cable lengths and measurements of the cable angular positions. A general cable mechanism with an end-effector moving in three-dimensional space is considered. It is constrained by m cables attached by reels to the fixed frame, as shown schematically in Fig. 3. The position of the i^{th} anchor point A_i is defined by vector $\mathbf{a}_i$ expressed in the fixed reference frame $\mathscr{F}$ originating at point O. Each anchor point has a corresponding fixed reference frame $\mathscr{A}_i$, which defines the angular sensor pose. The corresponding attachment point on the end-effector is defined by vector $\mathbf{r}_i$ expressed in the mobile reference frame $\mathscr{P}$. The origin of this latter frame is P, and its position with respect to O is represented by vector $\mathbf{p}$. The orientation of the mobile reference frame $\mathscr{P}$ with respect to the fixed reference frame $\mathscr{F}$ is defined by the rotation matrix $\mathbf{Q}$. Also, the orientation of each anchor point reference frame $\mathscr{A}_i$ with respect to the fixed reference frame $\mathscr{F}$ is defined by the rotation matrix $\mathbf{Q}_{Ai}$. It is important to note that cable elasticity and mass are considered negligible and are not accounted for in this model. The validity of this assumption is assessed in sec. VI.

A. Kinematics for cable length measurements

The length ρ_i of the i^{th} cable can then be written as

$$\rho_i^2 = \mathbf{u}_i^T \mathbf{u}_i = \| \mathbf{p} + \mathbf{Q}\mathbf{r}_i - \mathbf{a}_i \|^2, \tag{1}$$

with $\mathbf{u}_i$ defined in Fig. 3.

By differentiation and rearrangement of (1), the corresponding velocity equation is written as

$$\rho_i \dot{\rho}_i = (\mathbf{p} + \mathbf{Q}\mathbf{r}_i - \mathbf{a}_i)^T \dot{\mathbf{p}} + [(\mathbf{Q}\mathbf{r}_i) \times (\mathbf{p} + \mathbf{Q}\mathbf{r}_i - \mathbf{a}_i)]^T \boldsymbol{\omega} \tag{2}$$

where $\boldsymbol{\omega}$ stands for the angular velocity of the end-effector.

For m cables, this leads to the following first-order kinematic relationship

$$\mathbf{K}\dot{\boldsymbol{\rho}} = \mathbf{J}_1\mathbf{t}, \tag{3}$$

where

$$\dot{\boldsymbol{\rho}} = [\dot{\rho}_1, \cdots, \dot{\rho}_m]^T \quad , \quad \mathbf{t} = \left[\dot{\mathbf{p}}^T, \boldsymbol{\omega}^T\right]^T,$$

and

$$\mathbf{J}_1 = [\mathbf{c}_1^T, \cdots, \mathbf{c}_m^T]^T, \quad \mathbf{K} = \text{diag}[\rho_1, \cdots, \rho_m], \tag{4}$$

where $\mathbf{c}_i$ is a six-dimensional vector defined as

$$\mathbf{c}_i = \begin{bmatrix} (\mathbf{p} + \mathbf{Q}\mathbf{r}_i - \mathbf{a}_i) \\ (\mathbf{Q}\mathbf{r}_i) \times (\mathbf{p} + \mathbf{Q}\mathbf{r}_i - \mathbf{a}_i) \end{bmatrix}. \tag{5}$$

B. Kinematics for cable angular position measurements

The first-order kinematic relationship between the pose and the angular position sensor can be obtained in a similar way. The angular position of each cable in their respective reference frame can be expressed as

$$\begin{bmatrix} \tan(\theta_i) \\ \tan(\phi_i) \end{bmatrix} = \begin{bmatrix} \frac{u_y}{u_z} \\ \frac{u_x}{u_z} \end{bmatrix}, \tag{6}$$

where $[u_x\ u_y\ u_z]^T = [\mathbf{u}_i]_{\mathscr{A}_i}$ expressed in its corresponding referential frame $\mathscr{A}_i$.

By differentiation and rearrangement of (6), the velocity equation can be written as

$$\begin{bmatrix} \dot{\theta}_i \\ \dot{\phi}_i \end{bmatrix} = \begin{bmatrix} 0 & \frac{u_{iz}}{u_{iy}^2 + u_{iz}^2} & -\frac{u_{iy}}{u_{iy}^2 + u_{iz}^2} \\ \frac{u_{iz}}{u_{ix}^2 + u_{iz}^2} & 0 & -\frac{u_{ix}}{u_{ix}^2 + u_{iz}^2} \end{bmatrix} \dot{\mathbf{u}}_i \tag{7}$$

expressed in its corresponding referential frame $\mathscr{A}_i$.

By differentiation of the loop closure equation

$$\mathbf{u}_i = \mathbf{p} + \mathbf{Q}\mathbf{r}_i - \mathbf{a}_i, \tag{8}$$

the velocity equation

$$\dot{\mathbf{u}}_i = \dot{\mathbf{p}} + [\boldsymbol{\omega}]_\times \mathbf{Q}\mathbf{r}_i, \tag{9}$$

can be obtained, where $[\boldsymbol{\omega}]_\times$ is the skew symmetric matrix

$$\begin{bmatrix} 0 & -\omega_z & \omega_y \\ \omega_z & 0 & -\omega_x \\ -\omega_y & \omega_x & 0 \end{bmatrix}. \tag{10}$$

By rearranging (9),

$$\dot{\mathbf{u}}_i = \begin{bmatrix} \mathbf{1} & [\mathbf{Q}\mathbf{r}_i]_\times^T \end{bmatrix} \mathbf{t}, \tag{11}$$

with $\mathbf{1} \in \mathbb{R}^{3\times3}$ being the identity 3×3 matrix. Inserting (11) in (7) expressed in the referential frame $\mathscr{A}_i$ gives

$$\begin{bmatrix} \dot{\theta}_i \\ \dot{\phi}_i \end{bmatrix} = \mathbf{D}_i\mathbf{t} \tag{12}$$

where

$$\mathbf{D}_i = \begin{bmatrix} 0 & \frac{u_{iz}}{u_{iy}^2+u_{iz}^2} & -\frac{u_{iy}}{u_{iy}^2+u_{iz}^2} \\ \frac{u_{iz}}{u_{ix}^2+u_{iz}^2} & 0 & -\frac{u_{ix}}{u_{ix}^2+u_{iz}^2} \end{bmatrix} \mathbf{Q}_{Ai}^{-1} \begin{bmatrix} \mathbf{1} & [\mathbf{Q}\mathbf{r}_i]_\times^T \end{bmatrix}. \tag{13}$$

For m cables, the kinematic relationship is

$$\dot{\boldsymbol{\psi}} = \mathbf{J}_2\mathbf{t} \tag{14}$$

where

$$\dot{\boldsymbol{\psi}} = [\dot{\theta}_1, \dot{\phi}_1, \cdots, \dot{\theta}_m, \dot{\phi}_m]^T \tag{15}$$

and

$$\mathbf{J}_2 = [\mathbf{D}_1^T, \cdots, \mathbf{D}_m^T]^T. \tag{16}$$

C. Combined kinematics

The full first-order kinematic relationship can then be obtained from (3) and (14) and becomes

$$\begin{bmatrix} \mathbf{K} & \mathbf{0} \\ \mathbf{0} & \mathbf{1} \end{bmatrix} \begin{bmatrix} \dot{\boldsymbol{\rho}} \\ \dot{\boldsymbol{\psi}} \end{bmatrix} = \begin{bmatrix} \mathbf{J}_1 \\ \mathbf{J}_2 \end{bmatrix} \mathbf{t}. \tag{17}$$

When dealing with mechanism with orientation capabilities, Euler angles time derivatives ($\dot{\mathbf{e}}$) can be mapped linearly to angular velocities by a matrix $\mathbf{S}$ defined as $\boldsymbol{\omega} = \mathbf{S}\dot{\mathbf{e}}$. The linear relationship for small displacement can then be written

$$\begin{bmatrix} \mathbf{K} & \mathbf{0} \\ \mathbf{0} & \mathbf{1} \end{bmatrix} \begin{bmatrix} \Delta\boldsymbol{\rho} \\ \Delta\boldsymbol{\psi} \end{bmatrix} = \begin{bmatrix} \mathbf{J}_1 \\ \mathbf{J}_2 \end{bmatrix} \begin{bmatrix} \Delta\mathbf{p} \\ \mathbf{S}\Delta\mathbf{e} \end{bmatrix}. \tag{18}$$

IV. Sensor Fusion

The robot pose can be obtained independently by the cable length measurements or the cable angular position measurements. In this section, a fusion algorithm is developed which uses both of these measurements as input. For an unknown true pose $\mathbf{x}$, the best pose estimate $\hat{\mathbf{x}}$ is the one that minimizes $\Delta\mathbf{x} = \mathbf{x} - \hat{\mathbf{x}}$. The problem to solve is common in sensor fusion and can be written as

$$\underset{\hat{\mathbf{x}}}{\text{minimize}} \quad \left\| \mathbf{W} \left(\begin{bmatrix} \hat{\boldsymbol{\rho}}^T & \hat{\boldsymbol{\psi}}^T \end{bmatrix}^T - h(\hat{\mathbf{x}}) \right) \right\|_2^2, \tag{19}$$

where $\hat{\boldsymbol{\rho}}$ and $\hat{\boldsymbol{\psi}}$ are measurements from the sensor, $h(\hat{\mathbf{x}})$ is the inverse kinematics of the mechanism and $\mathbf{W}$ is a weight matrix. For most parallel mechanisms $h(\hat{\mathbf{x}})$ is easily derived from (1) and (6). In most applications, (19) is solved numerically with an initial estimation stemming from the previous pose. The choice of the weight matrix $\mathbf{W}$ is of major importance. In stochastic sensor theory [25], this matrix is chosen as the inverse of the covariance matrices. It is expressed as

$$\mathbf{W} = \text{diag}\left([\alpha_\rho\sigma_{\rho1}, \cdots, \alpha_\rho\sigma_{\rho m}, \alpha_\psi\sigma_{\psi1}, \cdots, \alpha_\psi\sigma_{\psi m}]\right)^{-1}, \tag{20}$$

where α_ρ and α_ψ are added weights that normalize the difference in measure units. This method is still applicable here even if the readings are not picked from a Gaussian distribution. An estimate of the absolute error on each sensor can be used instead of the variance of the sensor measurements.

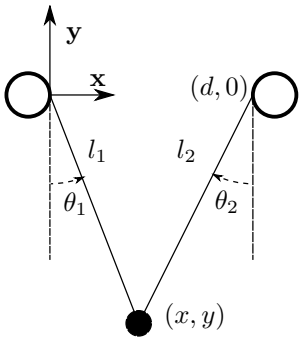

Fig. 4: Geometric model of the simulated CDPM.

V. Simulation

As previously detailed in the paper, the robot pose can be obtained 1) with the cable length as input, 2) with the cable direction as input and 3) with a fusion algorithm using both the cable length and direction. In this section, the theoretical accuracy of these methods is compared by simulation. To assess the accuracy of a pose estimate, it is possible to bound the pose error of the estimator $\hat{\mathbf{x}}$ by projection of the sensor articular errors in the end effector space. By linearising at $\hat{\mathbf{x}}$, (18) is used to compute a region containing $\Delta\mathbf{x}$ as

$$\Delta\underline{\boldsymbol{\tau}} \leq \mathbf{A}\Delta\mathbf{x} \leq \Delta\bar{\boldsymbol{\tau}} \tag{21}$$

with

$$\mathbf{A} = \begin{bmatrix} \mathbf{K} & \mathbf{0} \\ \mathbf{0} & \mathbf{1} \end{bmatrix}^{-1} \begin{bmatrix} \mathbf{J}_1 \\ \mathbf{J}_2 \end{bmatrix}, \tag{22}$$

where $\Delta\bar{\boldsymbol{\tau}}$ and $\Delta\underline{\boldsymbol{\tau}}$ represents the upper and lower error boundaries in articular space. This is mathematically expressed as

$$\Delta\underline{\boldsymbol{\tau}} \leq \begin{bmatrix} \boldsymbol{\rho} \\ \boldsymbol{\psi} \end{bmatrix} - \begin{bmatrix} \hat{\boldsymbol{\rho}} \\ \hat{\boldsymbol{\psi}} \end{bmatrix} \leq \Delta\bar{\boldsymbol{\tau}}. \tag{23}$$

A planar two DOFs CDPM is used as illustrated in Fig. 4 for the simulation. The inverse kinematics for this mechanism is

$$\begin{bmatrix} l_1 \\ l_2 \\ \theta_1 \\ \theta_2 \end{bmatrix} = h(\mathbf{x}) = \begin{bmatrix} \sqrt{x^2+y^2} \\ \sqrt{(d-x)^2+y^2} \\ \tan^{-1}\left(\dfrac{x}{-y}\right) \\ \tan^{-1}\left(\dfrac{d-x}{-y}\right) \end{bmatrix}, \tag{24}$$

with the pose being $\mathbf{x} = \begin{bmatrix} x & y \end{bmatrix}^T$. The expression of the first order kinematic relationship $\mathbf{A}$ can be expressed as

$$\mathbf{A} = \begin{bmatrix} \dfrac{x}{\sqrt{x^2+y^2}} & \dfrac{y}{\sqrt{x^2+y^2}} \\ \dfrac{-d+x}{\sqrt{(d-x)^2+y^2}} & \dfrac{y}{\sqrt{(d-x)^2+y^2}} \\ \dfrac{-1}{y(1+\frac{x^2}{y^2})} & \dfrac{x}{y^2(1+\frac{x^2}{y^2})} \\ \dfrac{1}{y(1+\frac{(d-x)^2}{y^2})} & \dfrac{d-x}{y^2(1+\frac{(d-x)^2}{y^2})} \end{bmatrix}. \tag{25}$$

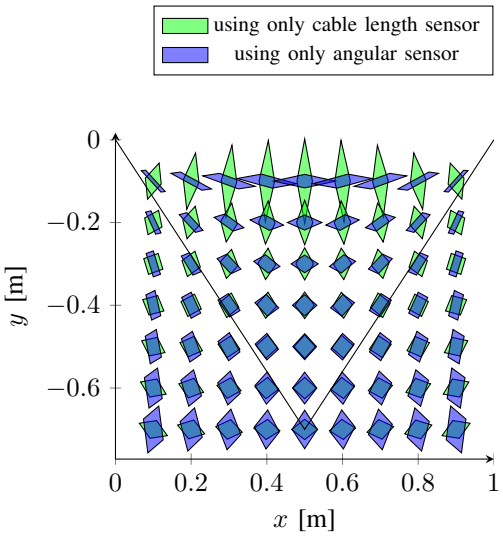

Fig. 5: Limits of pose error while using measurements from lengths and angles. Errors are ± 0.02 m in cable length and $\pm 1.8°$ in angular measurement. Center point of each region is the simulated true pose. Cable anchor points are at $[0, 0]$ and $[1, 0]$.

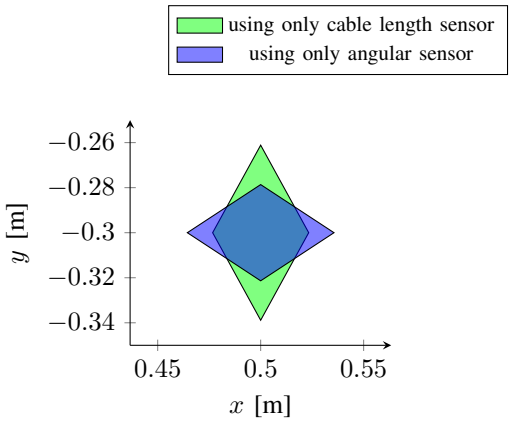

Fig. 6: Portion of Fig. 5 at pose $x = 0.5m$ and $y = -0.3m$.

The pose estimation error bounds is shown in Fig. 5 both by using the cable length as input and the angular position as input. These bounds are obtained from eq. (21). The intersection of both region represents the error while using data fusion with both types of sensor. Those regions are traced for several points inside the workspace. The uncertainty on each sensor has been set to ± 2 cm for the cable lengths and to $\pm 1.8°$ for the angular measurements. Fig. 6 is a close-up of Fig. 5 for the case where $\mathbf{x} = \begin{bmatrix} 0.5 & -0.3 \end{bmatrix}^T$. In many places on the workspace, the intersection of the two regions is smaller than each of the two taken separately, which signifies a reduced error. From those figures, it can be noted that the benefits of using additional angular position sensors are most apparent when approaching the edges of the workspace where the measurement sensitivity of the cable length sensor is low. This happens when $\mathbf{J}_1$ is near a singularity, like in this example when $y \to 0$.

VI. Experiment

An experiment is devised to further benchmark the benefits of using angular position sensors on a real mechanism. The mechanism used for testing is shown in Fig. 1 and has the same architecture as the simulated one shown in Fig. 4. The experimentation is done by generating a quasi-static trajectory with the mechanism and by comparing the estimated pose obtained from three different sets of sensors relatively to a ground truth. The three different sets are : cable length measurements only, angular position sensor only and the combination of the two by using the sensor fusion algorithm. For the first two sets, the forward kinematic is used to get the estimated pose. The forward kinematic for this mechanism amount to the intersection of two circles for the cable length measurements and the intersection of two lines for the case of angular measurements. For the last set, the fusion method described in sec. IV is used. The ground truth is obtained with the help from an external measurement of the pose, which is performed by a vision system.

The experimental set-up is shown in Fig. 1. Two winches with incremental encoders are used in conjunction with two angular position sensors. Those are shown in the figure in the upper-left and upper-right corners of the frame. The end effector is a small mass of 115 g on which each cable is attached to the same point. The cable is light with a linear weight of 1.5 g/m. The cable is highly stiff for this purpose with a stiffness larger than 50 N/mm, since expected tension should not surpass 10 N. The external vision system, a VICON©, is also shown in Fig. 1. This system can track a marker in three dimensional space and has an accuracy in the order of a millimetre, given its calibration method and this particular installation. Incremental encoders used for cable length measurements have a resolution of 2048 per revolution and are coupled to a gearbox with a ratio of 5.9 giving a resolution of $0.03°$. Using a pulley with a radius of 25.4 mm, the resolution of the cable length is 0.013 mm. Given some backlash in the gearbox, some compliance in the winches and uncertainty in the initialization of the incremental encoders, the errors in measured length is in the order of one centimetre. As for the angular position sensor, the resolution of the encoders are 2000 counts per revolution and are directly attached to the guides, which gives an angular resolution of $0.18°$. Given uncertainty in the initialisation, an error in the order of two degrees is to be expected.

To assess the validity of the rigid and massless cables simplification, the catenary equation presented in [10] are used to compute the shape of a corresponding extensible and hefty cable modelled with the characteristic of the cable used in the experiment. At a worst case scenario (the end-effector near one of the anchor point coupled with a low tension), an error of $0.21°$ is observed for the angle of departure at the anchor's point between the two models. As for the stiffness, with a maximum tension of 10 N an error of less than 0.5 mm can be expected. Both of those errors are within the margin of error of the measurements.

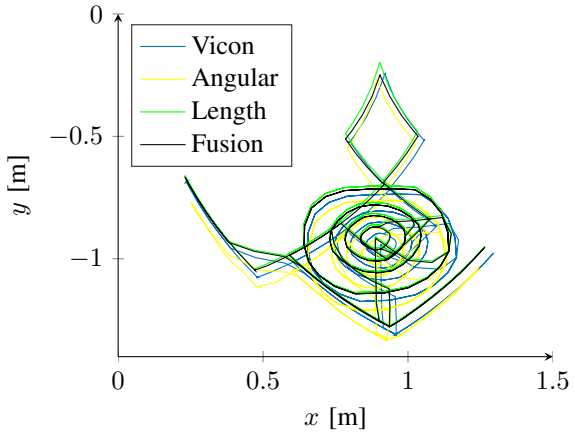

Fig. 7: Pose of the end-effector tracked by the VICON© and pose estimate by the cable length sensor only, the angular sensor only and sensor fusion

TABLE I: Observed error between the vision system and the pose estimate from the different sets of sensor

	rms error [cm]	max error [cm]
Cable length only	3.92	5.01
Angular sensor only	4.18	10.52
Fusion	3.19	4.16

During the initialization phase, each sensor is referenced to a common frame of reference by open loop measurements to allow comparison of each pose estimation with each other. While this method is representative of the use of the mechanism without external measurements like the VICON© system, it can be expected to have an offset bias with the external measure. This is observed in Fig. 7 where the VICON© measurement of the pose has an offset with the pose estimators.

Table I presents the root-mean-square (rms) error between the pose estimate of each set of sensors to the externally measured pose. The maximal error between the estimate and the measured pose is also presented.

It can be observed that the error obtained from the angular position sensors is higher than the estimate obtained from the cable length sensors but the fusion of both measurements presents better result. A diminution of the rms error of 19% is observed between the cable length and the fusion estimate along with a diminution of 17% on the maximal error.

From the same set of data, a realignment of the VICON© measurement can be done in post-processing so that each estimate starts at the same position. This position is chosen to represent a real world implementation, where the initial position is known. The graph of Fig. 8 is obtained by removing via post-processing the offset bias caused by uncertainties in the calibration phase. The corresponding rms and maximum errors are presented in Table II.

It can then be observed that the benefits becomes a reduction by 18% of the rms error and a reduction by 45% of the maximum error.

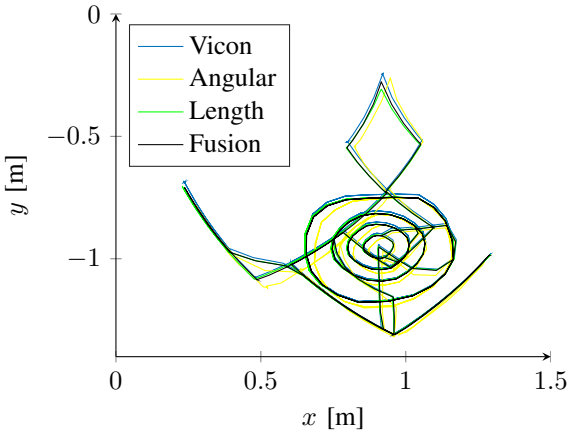

Fig. 8: Pose of the end-effector tracked by the VICON© and pose estimate by the cable length sensor only, the angular sensor only and sensor fusion after post-processing

TABLE II: Observed error between the vision system and the pose estimate from the different sets of sensor with post processing calibration

	rms error [cm]	max error [cm]
Cable length only	1.52	6.32
Angular sensor only	3.90	12.3
Fusion	1.25	3.48

VII. Conclusion

This paper proposed to use cable angle position sensors in addition to cable length measurements in order to improve the accuracy of cable driven parallel mechanisms. The angular position sensor was first presented. The kinematic equations were then individually obtained by considering only the cable length measurements and then with the cable angle position measurements. A data fusion scheme combining these two types of measurements was then presented. Finally, simulations and experiments were presented in order to assess the benefits of using cable angle position sensors on the accuracy of CDPMs.

The results show an improved accuracy, especially in low-sensitivity robot configurations, which often occur near singularities. Indeed, near these positions, the error boundaries are high but each type of sensor sensitivity is different, so that the fusion of their measurements leads to an improved overall accuracy.

Future work will focus on determining the benefits of using cable angle sensors with more complex CDPMs. Additionally, the benefits of using cable angle sensors in order to discriminate between multiple solutions of the forward kinematics will be explored. Indeed, strategic placement of additional sensor on a parallel mechanism can lead to a closed-form resolution of the forward kinematics even for complex mechanisms [7].

ACKNOWLEDGMENT

This work was supported by The Natural Sciences and Engineering Research Council of Canada (NSERC) as well as the Fonds de recherche Nature et technologie Québec (FRQNT) 2015-PR-180481.

References

[1] A. Fortin-Cote, P. Cardou, and C. Gosselin, "An admittance control scheme for haptic interfaces based on cable-driven parallel mechanisms," in *2014 IEEE International Conference on Robotics and Automation (ICRA)*, may, pp. 819–825.

[2] C. Gosselin, "Cable-driven parallel mechanisms: state of the art and perspectives," *Mechanical Engineering Reviews*, vol. 1, no. 1, 2014.

[3] L. L. Cone, "Skycam: an aerial robotic camera system," *BYTE*, vol. 10, pp. 122–132, 1985.

[4] J. Albus, R. Bostelman, and N. Dagalakis, "The NIST SPIDER, a robot crane," *Journal of research of the NIST*, vol. 97, no. 3, 1992.

[5] N. Riehl, M. Gouttefarde, S. Krut, C. Baradat, and F. Pierrot, "Effects of non-negligible cable mass on the static behavior of large workspace cable-driven parallel mechanisms," in *2009 IEEE International Conference on Robotics and Automation*, pp. 2193–2198.

[6] A. J. Patel and K. F. Ehmann, "Calibration of a hexapod machine tool using a redundant leg," *International Journal of Machine Tools and Manufacture*, vol. 40, no. 4, pp. 489–512, mar 2000.

[7] J. P. Merlet, "Closed-form resolution of the direct kinematics of parallel manipulators using extra sensor data," in *Proceedings IEEE International Conference in Robotics and Automation*, 1993, pp. 200–204.

[8] R. Chellal, L. Cuvillon, and E. Laroche, "A Kinematic Vision-Based Position Control of a 6-DoF Cable-Driven Parallel Robot," in *Cable Driven Parallel Robots*, ser. Mechanisms and Machine Science, T. Bruckmann and A. Pott, Eds. Berlin, Heidelberg: Springer Berlin Heidelberg, 2015, vol. 12, pp. 213–225.

[9] T. Dallej, M. Gouttefarde, N. Andreff, R. Dahmouche, and P. Martinet, "Vision-based modeling and control of large-dimension cable-driven parallel robots," in *2012 IEEE/RSJ International Conference on Intelligent Robots and Systems*, pp. 1581–1586.

[10] Dinh Quan Nguyen, M. Gouttefarde, O. Company, and F. Pierrot, "On the simplifications of cable model in static analysis of large-dimension cable-driven parallel robots," in *2013 IEEE/RSJ International Conference on Intelligent Robots and Systems*, nov, pp. 928–934.

[11] W. Kraus, V. Schmidt, P. Rajendra, and A. Pott, "Load identification and compensation for a Cable-Driven parallel robot," in *2013 IEEE International Conference on Robotics and Automation*, pp. 2485–2490.

[12] P. Cardou, S. Bouchard, and C. Gosselin, "Kinematic-Sensitivity Indices for Dimensionally Nonhomogeneous Jacobian Matrices," *IEEE Transactions on Robotics*, vol. 26, no. 1, pp. 166–173, 2010.

[13] S. Kawamura, W. Choe, S. Tanaka, and S. Pandian, "Development of an ultrahigh speed robot FALCON using wire drive system," in *Proceedings of 1995 IEEE International Conference on Robotics and Automation*, vol. 1, pp. 215–220.

[14] J. Perret and L. Dominjon, "The INCA 6D: a Commercial Stringed Haptic System Suitable for Industrial Applications," in *SPIDAR Anniversary Symposium*, 2009.

[15] J.-b. Izard, M. Gouttefarde, M. Michelin, O. Tempier, and C. Baradat, "A Reconfigurable Robot for Cable-Driven Parallel Robotic Research and Industrial Scenario Proofing," in *Cable-Driven Parallel Robots*, ser. Mechanisms and Machine Science, T. Bruckmann and A. Pott, Eds. Berlin, Heidelberg: Springer Berlin Heidelberg, 2013, vol. 12, pp. 135–148.

[16] M. A. Peshkin, "Non-contacting sensors," 2003. [Online]. Available: https://www.google.com/patents/US6668668

[17] O.-s. Kim, K.-s. Hong, and S.-k. Sul, "Anti-sway control of container cranes: inclinometer, observer, and state feedback," *International Journal of Control, Automation, and Systems*, vol. 2, no. 4, pp. 435–449, 2004.

[18] J. Huang, X. Xie, and Z. Liang, "Control of Bridge Cranes With Distributed-Mass Payload Dynamics," *IEEE/ASME Transactions on Mechatronics*, vol. 20, no. 1, pp. 481–486, 2015.

[19] K. L. Sorensen, W. Singhose, and S. Dickerson, "A controller enabling precise positioning and sway reduction in bridge and gantry cranes," *Control Engineering Practice*, vol. 15, no. 7, pp. 825–837, 2007.

[20] G. Stepan, A. Toth, L. Kovacs, G. Bolmsjo, G. Nikoleris, D. Surdilovic, A. Conrad, A. Gasteratos, N. Kyriakoulis, D. Chrysostomou, R. Kouskouridas, J. Canou, T. Smith, W. Harwin, R. Loureiro, R. Lopez, and M. Moreno, "ACROBOTER: a ceiling based crawling, hoisting and swinging service robot platform," *Proceedings of beyond gray droids: domestic robot design for the 21st century workshop at HCI 2009*, p. 2.

[21] S. Kahlman, "Arrangement for controlling the direction of movement of a load hoist trolley," 1994. [Online]. Available: http://www.google.com/patents/US5350075

[22] S. Ohtomo and T. Murakami, "Estimation method for sway angle of payload with reaction force observer," in *13th International Workshop on Advanced Motion Control*, 2014, pp. 581–585.

[23] A. Lecours, S. Foucault, T. Laliberte, C. Gosselin, B. Mayer-St-Onge, D. Gao, and R. J. Menassa, "Movement system configured for moving a payload in a plurality of directions," 2015. [Online]. Available: https://www.google.com/patents/US8985354

[24] A. Campeau-Lecours, S. Foucault, T. Laliberte, B. Mayer-St-Onge, and C. Gosselin, "A Cable-Suspended Intelligent Crane Assist Device for the Intuitive Manipulation of Large Payloads," *IEEE/ASME Transactions on Mechatronics*, vol. 21, no. 4, pp. 2073–2084, aug 2016.

[25] H. Stark and J. W. Woods, "Probability, random processes, and estimation theory for engineers," *Englewood Cliffs: Prentice Hall, 1986*, vol. 1, 1986.